# Interaction Analyses of hTAAR1 and mTAAR1 with Antagonist EPPTB

Siyan Liao[a, §], Michael James Pino Jr.[b, §], Catherine A. Deleon[b], Maurice Lindner-Jackson[b] and Chun Wu[b,*]

[a] Key Laboratory of Molecular Target & Clinical Pharmacology, School of Pharmaceutical Sciences, Guangzhou Medical University, Guangzhou, 511436, China

[b] Department of Chemistry and Biochemistry, Rowan University, 201 Mullica Hill Rd, Glassboro NJ 08028

[§] Co-first author

* Corresponding author

*E-mail address:* wuc@rowan.edu (Chun Wu)

**Abstract**

Trace amine-associated receptor 1 (TAAR1) plays a critical role in regulating monoaminergic activity. EPPTB is the only known selective potent antagonist of the mouse (m) TAAR1 presently, while it was shown to be weak at antagonizing human (h) TAAR1. The lack of high-resolution structure of TAAR1 hinders the understanding of the differences in the interaction modes between EPPTB and m/hTARR1. The purpose of this study is to probe these interaction modes using homology modeling, molecular docking, molecular dynamics (MD) simulations, and molecular mechanics-generalized Born surface area (MM-GBSA) binding energy calculations. Eight populated conformers of hTAAR1-EPPTB complex were observed during the MD simulations and could be used in structure-based virtual screening in future. The MM-GBSA binding energy of hTAAR1-EPPTB complex (-96.5 kcal/mol) is larger than that of mTAAR1-EPPTB complex (-106.7 kcal/mol), which is consistent with the experimental finding that EPPTB has weaker binding affinity to hTAAR1. The several residues in binding site of hTAAR1 ($F154^{4.56}$, $T194^{5.42}$ and $I290^{7.39}$) are different from these of mTAAR1 ($Y153^{4.56}$, $A193^{5.42}$ and $Y287^{7.39}$), which might contribute to the binding affinity difference. Our docking analysis on another hTAAR1 antagonist Compound **3** have found that 1). this compound binds in different pockets of our mTAAR1 and hTAAR1 homology models with a slightly stronger binding affinity to hTAAR1; 2). both antagonists bind to a very similar pocket of hTAAR1.

**Keywords:** TAAR1; EPPTB; homology modeling; molecular docking; MD simulation

---

*Abbreviations:* mTAAR1, mouse trace amine-associated receptor; hTAAR1, human trace amine-associated receptor; EPPTB, N-(3-ethoxy-phenyl)-4-pyrrolidin-1-yl-3-trifluoromethyl-benzamide; TM, transmembrane; ICL, intracellular loop; ECL, extracellular loop; SID, simulation interaction diagram; RMSD, root mean square deviation; PRCG, Polak-Ribier conjugate gradient.

## 1. Introduction

Trace amine-associated receptors (TAARs) belongs to aminergic receptors, a family of class A (rhodopsin-like) G-protein coupled receptor (GPCR)[1, 2] and consists of six functional human TAARs (hTAARs). TAAR1, the best characterized TAAR so far, is one human variant that is non-selectively activated by endogenous trace amines (p-tyramine, p-octopamine, tryptamine, β-phenylethylamine) and classical monoamine neurotransmitters (dopamine, histamine, norepinephrine, serotonin)[1-3]. TAAR1 is broadly expressed in the brain and peripheral nervous system, especially within the monoaminergic systems, such as dopaminergic and serotonergic circuitries[4]. TAAR1 activation acts as a rheostat of the dopaminergic, glutamatergic, and serotonergic neurotransmission[5] and has been considered as a novel promising therapeutic target for psychiatric and neurodegenerative disorders like schizophrenia, depression, and addiction[6, 7]. However, the detailed working mechanisms of the TAAR1 still remain elusive. The activation of TAAR1 not only activates $G_s$-protein signaling pathway to stimulate the secondary messenger cyclic adenosine monophosphate (cAMP) production, but it also activates the G protein-gated inwardly rectifying $K^+$ (GIRK) channels and the β-arrestin 2 pathway[8, 9]. The availability of a selective TAAR1 agonists and antagonists, which do not interact with other monoamine receptors, is critical for the identification of specific TAAR1-mediated signaling mechanisms.

Recently, a number of highly selective TAAR1 agonists and partial agonists with different chemical scaffolds have been developed and synthesized[10-17]. Cichero *et al.* proposed some activated hTAAR1's key residues responsible for its agonist recognition and identified several agonists and one antagonist for the hTAAR1 by using homology modelling, docking and virtual screening methods[18, 19]. However, the development of the selective TAAR1 antagonists has still been a challenge. So far, the only highly potent and selective mouse TAAR1 (mTAAR1) antagonist (or inverse agonist) EPPTB (N-(3-ethoxy-phenyl)-4-pyrrolidin-1-yl-3-trifluoromethyl-benzamide, **Fig. S1**) has been identified[20, 21]. The EPPTB can selectively dampen the activation of its target receptor mTAAR1 and at the same time it does not interact with other monoamine receptors

during the process. Furthermore, the EPPTB can increase the firing frequency of the dopamine neurons and the affinity of dopamine to the D2 receptor, but it will block the TAAR1-mediated activation of an inwardly rectifying $K^+$ current[20].

Although EPPTB showed strong antagonism activity with a strong binding to mTAAR1 (binding affinity: $K_i$ = 0.0009 μM), it showed weak antagonism activity with a very weak binding to hTAAR1 ($K_i$ >5 μM)[21]. The cause of this occurrence is still poorly understood and thus has hindered the advancement and development of using the properties of EPPTB for mental illness treatment. In addition, EPPTB's poor pharmacokinetic properties also limits its usefulness in vivo[20]. However, we still chose EPPTB for this study because it is the only known selective antagonist against the mTAAR1 receptor.

In fact, the unavailability of a high-resolution crystal structure of the TAAR1 structure and the limitation on the use of EPPTB have significantly blocked the progress in studying the basic biological functions of hTAAR1 and developing better selective antagonists of hTAAR1[6]. Therefore, insights into the interactions between EPPTB and hTARR1 needs to be explored with the emphasis of developing better selective hTAAR1 antagonists which are urgently needed.

In-silico techniques are getting more and more popular in deciphering molecular mechanics of biological systems [22, 23]and in screening drug candidates [7] due to the improved predication power and low cost[24, 25]. Homology modeling is a procedure that builds a previously unknown three-dimensional (3D) protein structure according to its known sequence by using one or several known 3D structures of related family members as templates. Molecular docking is an approach to predict the interaction modes between a ligand and its receptor at the atomic level. Molecular dynamics (MD) simulation is a useful tool to investigate the structural dynamics of a bimolecular system to reveal its function and mechanism of action. The MM-GBSA binding energy calculation can be used to evaluate the binding affinity to estimate whether a binding mode is stable or not. Therefore, various computational methods, which included homology modeling, molecular docking, MD

simulation and MM-GBSA binding energy calculation, could acquire potential binding modes between the ligand and the receptor to offer useful information for understanding the interaction mechanism and directing the design of new compounds.[26-32]

In this study, homology modeling, molecular docking, and molecular dynamics (MD) simulation with molecular mechanics generalized Born surface area (MM-GBSA) binding free energy calculation were carried out to investigate the interactions of EPPTB in the binding pockets of the receptors, mTAAR1 and hTAAR1, and understand the reasons for their activity differences in helping to design a novel hTAAR1 antagonist. Using all atom MD simulations, the differences between hTAAR1 and mTAAR1 complexes were analyzed in binding energies, ligand poses, residue interactions, receptor conformational changes and MM-GBSA binding free energy. The aim of the study is to reveal the detailed structural and dynamic insights of the interaction mechanisms between EPPTB and m/hTARR1, and to generate preferred EPPTB-bound hTARR1 conformations for screening its new antagonist compounds with high binding affinity to hTAAR1 in future studies.

## 2. Computational materials and methods

### Homology modeling and preparation of protein structures (inactive hTAAR1 and m/hTAAR1)

So far, the crystal structure of any TAAR1 has not been solved. The advanced homology modeling tool in Maestro 10.3[33, 34] was used to build the inactive TAAR1 homology models. This tool is a comparative modeling used to create accurate homologous structure for structure-based research, where the backbone model is generated by threading and fold recognition techniques in cases of low or no-sequence identity[29, 31, 35-38]. The FASTA sequence of hTAAR1 (Q96RJ0) and mTAAR1 (Q923Y8) shown in **Fig. S2** was taken from uniProt [35]. First, a blast search was carried out to find a list of homology protein structures of hTAAR1 from the protein structure databank. The blast search results are shown in Table S1 which describes the protein, pdb id, E-value, score, ligand name, ligand type, species, etc. The inactive structure of the D2 Dopamine receptor (pdb id: 6CM4) was selected as the structure template to build the inactive hTAAR1 homology model because of the high score

of 288 and the presence of an antagonist found within the complex with the receptor. Using the D2 dopamine receptor, the inactive hTAAR1 homology model was built, then the hTAAR1 homology model was prepared, optimized and minimized with an optimized potential for liquid simulations 3 (OPLS3) force field[33] using the protein preparation wizard[34] implemented in Maestro 10.3. Subsequently, the inactive mTAAR1 homology model was built using the same procedure as hTAAR1. Finally, the inactive mTAAR1 homology model was also optimized and minimized in protein preparation wizard[34].

**Validation of the mTAAR1 and hTAAR1 homology models**

The m/hTAAR1 homology models were inspected by a protein check analysis and the Ramachandran plots. A protein check analysis was carried out to inspect the quality of the mTAAR1 and hTAAR1 homology models before and after energy minimization (**Figure S3A**), and it showed slight improvement after energy minimization. The potential energy of the mTAAR1 before energy minimization, 11861.6 kcal/mol and after energy minimization, -10676.6 kcal/mol, which suggests that it has removed the bad contacts that were found within the structure. The potential energy of the hTAAR1 before energy minimization, 1126.13 kcal/mol and after energy minimization, -10141.0 kcal/mol which also suggests the removal of bad contacts. Furthermore, the Ramachandran plots of the mTAAR1 and hTAAR1 homology models before and after minimization (**Figure S3B**) show that most of the black dots which represent amino acid residues are located within the red regions being sterically favorable regions for alpha-helix and beta-sheet conformations without spatial clashes. There is a smaller group of black dots located within the yellow regions being sterically allowed regions. Whereas only one or two residues are located within white regions being sterically disallowed regions. Therefore, the inactive homology structures of mTAAR1 and hTAAR1 built by us are reasonable.

**The preparation of ligand (EPPTB and Compound 3)**

The canonical SMILE code for EPPTB was acquired from PubChem so that the two-dimensional (2D) structure of the ligand could be constructed using the 2D sketcher in Maestro and correct any flaws that were

observed in the structure. Compound 3 was manually drawn using the 2D sketcher. The 2D structure of EPPTB and Compound 3 were converted to the 3D structures by saving them through the 2D sketcher to the workspace in Maestro. Then the ionization/tautomeric state of the ligand was generated at a pH=7 using Epik (an empirical pKa prediction program) calculation[34]. Finally, the optimization of EPPTB and Compound 3 were done to minimize the potential energy to relax any of the bad contacts that would be on the ligand using default parameters (Force field: OPLS3; Method: PRCG; Maximum iterations: 2500; Gradient convergence threshold: 0.5). Because EPPTB and Compound 3 is a small molecule, using the default parameters for minimization is entirely enough to reach our goal of optimizing them. As a result, the optimal molecular structure of EPPTB and Compound was obtained for the next docking step.

**Glide XP docking of EPPTB and Compound 3**

When the sitemap was created by using the binding site detection of Maestro, the maximum number of reported sites was set to be 5; each reported site contained at least 15 site points; the distance between site points was set to be 4Å. The first site was taken as the binding site of each protein, a grid box center was set at the center of the first site by picking one site point, and the Glide extra precision (XP) docking function[36, 37] was selected. Then the ligand (EPPTB and Compound3) was respectively docked to the prepared mTAAR1 and hTAAR1 homology models. These complexes were used as input structures for following induced fit docking.

**Induced fit dockings of EPPTB and Compound 3**

The induced fit docking is an ideal method to predict a ligand's binding conformations and associated structural changes in the receptor. Automatic Trim side chains based on B-factor was selected and the Van der Waals scaling factors of the receptor and ligand were set to be 0.7 and 0.5, and the maximum number of ligand pose was set to be 20. The implicit membrane model was used in refining the complex structure refinement including the residues within 4.0 Å of ligand and their sidechains. The Glide redocking was performed by using the extra precision (XP) docking scoring function[36, 37]. The ligand (EPPTB and Compound 3) was respectively

docked to the prepared mTAAR1 and hTAAR1 homology models. The ligand pose with the lowest XP score in the most abundant cluster was selected as the preferred docking conformation. The two induced fit docking complexes, mTAAR1-EPPTB and hTAAR1-EPPTB, were obtained as the initial structures for the following MD simulations.

**Setup of the two simulation systems**

Molecular dynamics (MD) simulation is a powerful tool to probe the conformational dynamics of a bimolecular system to understand its mechanism of action [38, 39]. Three independent MD simulations of 1.0 μs were carried out for each of the two preferred docking complexes, mTAAR1-EPPTB and hTAAR1-EPPTB, using the molecular dynamics program[40, 41] of Maestro 10.3. Each complex was placed in a biologically relevant membrane of phosphatidylcholine (POPC) lipids[42] and then dissolved in an orthorhombic water box which contained 10359 molecules of water for the hTAAR1 system and 10776 molecules of water for the mTAAR1 system with a buffer distance of 10Å using a simple point-charge (SPC) water model[43]. POPC is the most common lipid in animal cells [44], and POPC lipid bilayer is prototypical membrane model that has been widely benchmarked [45] and used in MD simulations of membrane proteins [46, 47], some of which were along with OPLS-AA (optimized potential for liquid simulations-all atom) force field [48, 49]. Then, the system was neutralized and salt was added at a concentration of 0.15 M NaCl, leading to30 sodium plus 39 chloride ions for the mouse TAAR1 system, and 29 sodium plus 39 chloride ions for the human TAAR1 system. The total number of atoms for the mTAAR1 and hTAAR1 system were 51357 atoms and 48883 atoms, and the system size with membrane in x, y, z directions for the mTAAR1 was ~93.18 Å, ~70.48 Å and ~106.15 Å and for the hTAAr1 system was ~92.67 Å, ~60.59 Å and ~107.65 Å, respectively. The whole mTAAR1 and hTAAR1 systems with membrane were shown in Fig S17. Lastly, OPLS3 force field[33] was used to simulate the receptor-ligand-lipid system.

**MD simulations of the two systems**

Using the Desmond module[50], for each modeled system they were relaxed to avoid any possible bad contacts and included the following stages: (1) each system was minimized with restraints on heavy atoms and

then without any restraints; (2) each system was gradually heated from 0 K to 300 K with $H_2O$ barrier and gradual restraining; (3) each system was simulated under the NPT ensemble (constant number of particles, P=1 bar and T=300 K) with $H_2O$ barrier and with heavy atoms restrained; (4) each system was simulated under the NPT ensemble with equilibration of solvent and lipids, then with protein heavy atoms annealing from 10.0 kcal/mol to 2.0 kcal/mol, then with $C_\alpha$ atoms restrained at 2 kcal/mol, and lastly for 1.5 ns with no restraints. After these relaxation steps, three independents ~1.0 μs production runs were conducted under the NPT ensemble (P=1 bar and T=310 K) for each system using default protocol. It is noted that the temperature was set to be 300 K (room temperature, or *in vitro* temperature) in the relaxation steps to simulate the environment outside the body, while the temperature was set to be 310 K (human body temperature, or *in vivo* temperature) in the production step to simulate the environment inside the body. During the MD simulations, the M-SHAKE algorithm[51] was used to constrain all covalent bonds including hydrogen atoms with a 2.0 fs time step; the k-space Gaussian split Ewald method[52] was used to handle long-range electrostatic interactions under a periodic boundary condition with a charge grid spacing of ~1 Å and the direct sum tolerance of $10^{-9}$; and the Van der Waals interactions were obeyed a uniform density approximation with a non-bonded cutoff of 9 Å. In addition, to reduce the overload of the calculation, non-bonded forces were calculated by using an r-RESPA[53] integrator in which the short range forces were updated every step and the long range forces were updated every three steps. For each system, the trajectories were saved at 50.0 ps intervals.

**Simulation interaction diagram (SID) analysis for the MD simulations**

Desmond SID tool, an automated post-MD-simulation analysis tool implemented in Maestro 10.3, is used to analyze protein-ligand interactions during the entire course of a MD simulation. The SID tool combines molecular analysis utilities with new plotting and visualization tools, obtaining unmatched insights into the atomic-level interactions between ligands and proteins. Simply, the automation of the SID analysis for the MD simulation gives the results, which are then organized in the SID panel with plots and diagrams for easy visualization of the information. Therefore, we choose the SID tool to simulate ligand-protein interactions in the

mTAAR1 and hTAAR1 systems. The data that were obtained from the simulations included: root mean square deviation (RMSD), ligand-protein contacts (hydrogen bond, hydrophobic, ionic, and water-bridge contacts), protein secondary structure element (SSE), root mean square fluctuation (RMSF), and Ligand Torsional Profiles**.**

**Trajectory clustering analysis for the MD simulations**

Desmond trajectory clustering tool[54] was used to group complex structures from the whole 3.0 μs MD trajectories of each system. A backbone RMSD matrix was used as a structural dissimilarity metric, and the average-linkage hierarchical clustering was selected as the clustering method with 2.5 Å merging distance cutoff. The centroid structure in the most abundant clusters was used to represent the structural family.

**MM-GBSA binding energy calculations for the last 100 ns MD simulations**

The binding energy calculations for snapshots from the last 100 ns simulation were calculated using the molecular mechanics generalized Born surface area (MM-GBSA) method with an implicit membrane which is a slab-shaped region with a low dielectric constant (~2). The MM-GBSA calculations adopted an OPLS3 force field [33], a VSGB 2.0 solvation model [25] and the default Prime protocol, where it first minimized the receptor alone, then the ligand alone, and finally the receptor-ligand complex. The total binding energy equation is: $\Delta G_{bind} = G_{complex} - (G_{ligand} + G_{receptor})$. To obtain a more detailed interaction information to understand the binding nature, the original interaction terms (coulombic, hydrogen bond, GB solvation, van der Waals, π-π stacking, self-contact, and lipophilic) were grouped into three major components: $\Delta E_{electrostatic}$, $\Delta E_{vdw}$ and $\Delta E_{lipophilic}$, and $\Delta G_{bind} = \Delta E_{electrostatic} + \Delta E_{vdw} + \Delta E_{lipophilic}$, where $\Delta E_{electrostatic} = E_{coulombic} + E_{H\text{-}bond} + E_{GB\text{-}solvation}$ and $\Delta E_{vdw} = E_{vdw} + E_{\pi\text{-}\pi\ stacking} + E_{self\text{-}contact}$. Since the same ligand binds to similar proteins, it will produce nearly the same entropy. Also, the entropy computation for the system with membrane of POPC lipids is very complex, so the entropy contribution was ignored in the study. It is noted that the entropy contribution is ignored in the MM-GBSA calculation. Thus, the MMGBSA binding free energy may overestimate the true binding affinity. However, if the entropic terms of

the same ligand to similar receptors are comparable, the entropic part of the binding free energy can be cancelled out and thus the MM-GBSA binding free energy difference can be used to estimate the relative binding affinity.

It is noted that, there is another popular binding energy calculation method called molecular mechanics-Poisson Boltzmann surface area (MM-PBSA)[55]. However, A previous study[23] showed that MM-GBSA performs better than MM-PBSA in predicting both correct binding poses and binding free energies for the examined protein-ligand systems. This study involved the comparison of two binding energies between mTARR1-EPPTB and hTARR1-EPPTB, and then screening new compounds will be performed by estimating binding energies in future. Therefore, we used the MM-GBSA method here.

**Results**

**The Docking showed slightly distinct EPPTB binding poses in mTAAR1 and hTAAR1, and the XP docking score have a higher negative value in mTAAR1-EPPTB complex.**

Since the high-resolution structure of the TAAR1 is unavailable, we built the inactive mTAAR1 and hTAAR1 structures by the homology modeling (**Fig. S4**). Then EPPTB was docked to the first site of mTAAR1 and hTAAR1 (**Fig. S5**), producing **13** and **12** ligand binding poses (**Fig. S6**), respectively. The binding pose with the lowest XP score in the most abundant cluster was selected as the preferred binding pose of EPPTB. The overlap of the two preferred binding poses is slightly different, with EPPTB moving up slightly in the mTAAR1 complex (**Fig. S7**). The EPPTB was suitably bond at the orthosteric binding site and had similar hydrophobic interactions with the surrounding residues (**Fig. S8**). In mTAAR1, the EPPTB formed hydrogen bonds with $W88^{ECL1}$, $H98^{3.28}$ and $D102^{3.32}$, and π-π interaction with $Y287^{7.39}$; but in hTAAR1, the EPPTB only formed a hydrogen bond with $D103^{3.32}$, and π-π interaction with $W264^{6.48}$ (Superscript numbers refer to Ballesteros-Weinstein residue numbering method for GPCRs[56]. As a result, the XP docking score of mTAAR1-EPPTB complex (-10.21 kcal/mol) is more negative than that of the hTAAR1-EPPTB complex (-8.16 kcal/mol), suggesting that the EPPTB binding affinity to mTAAR1 is stronger than to hTAAR1. It is well known that the

docking calculation could be rough, thus three independent ~1.0 μs MD simulations for each docking complex were further carried out to provide more accurate binding conformation.

**The RMSD values show that EPPTB in mTAAR1 was easier to reach stable state than it did in hTAAR1, indicating EPPTB in hTAAR1 fluctuated more strongly during the MD simulations.**

To check convergence of the MD simulations, the RMSD values of protein carbons ($C_\alpha$) and ligand in the two systems averaged over three independent MD simulations of 1.0 μs were calculated (**Fig. 1**). Relatively flat RMSD values were observed after 850 ns, indicating the two systems have reached steady states. In the two systems, protein RMSD values quickly reach ~5.0 Å during the first 150 ns, and then keep stable during the remaining 850 ns simulation. The ligand RMSD values of mTAAR1-EPPTB system gradually increase during the first 600 ns, and then reach a stable state at ~6.0 Å throughout the remaining 400 ns simulation. The ligand RMSD values of hTAAR1-EPPTB system are fluctuant during the first 850 ns, but finally reached a stable values at ~4.5 Å during the last 150 ns. Obviously, it took shorter relaxation time (~150 ns) for the receptors of m/hTARR1 to reach steady state than their ligand EPPTB, and it took shorter relaxation time (~150ns) for EPPTB in hTAAR1 to reach steady state than it did in mTAAR1 (~600 ns). On the other hand, the RMSD fluctuation of EPPTB in hTAAR1 is larger than that in mTAAR1during the MD simulations. The detailed protein and ligand RMSD plots of the m/hTAAR1 systems in each of the three independent trajectories of ~1.0 μs MD simulations are included in the supporting document (**Fig. S9**).

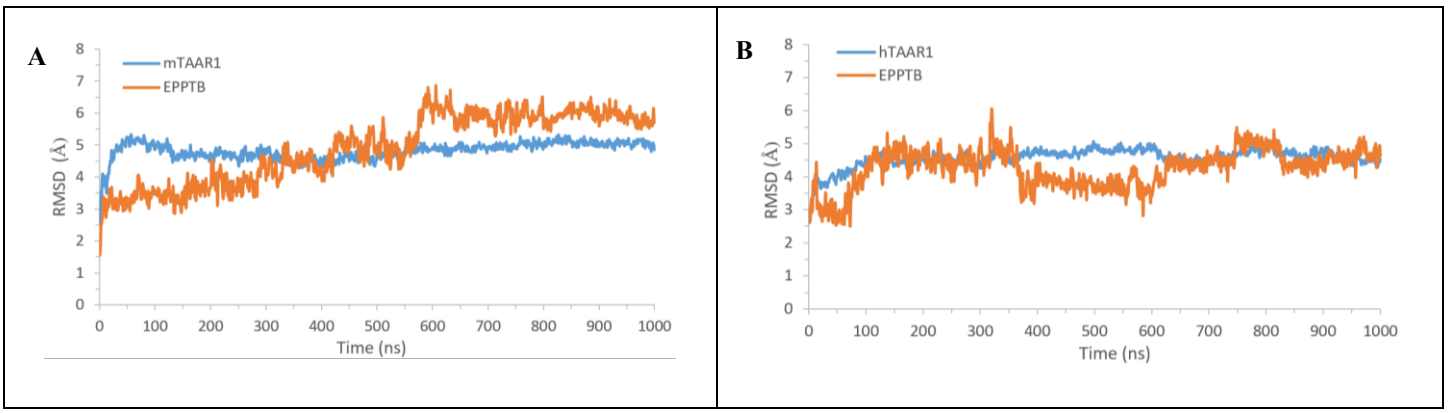


**Fig. 1.** RMSD values of receptor $C_\alpha$ (blue) and ligand EPPTB (orange) in the mTAAR1-EPPTB (**A**) and hTAAR1-EPPTB (**B**) systems averaged over three independent ~1.0 μs MD simulations.

**MM-GBSA binding energy data showed that the EPPTB binding affinity to mTAAR1 was stronger than to hTAAR1.**

To assess the binding affinity of EPPTB to mTAAR1 and hTAAR1, MM-GBSA binding energy calculations for the snapshots of the last 100 ns MD simulations were conducted and the results are listed in **Table 1**. The averaged van der Waals energy ($\Delta E_{vdw}$), electrostatic energy ($\Delta E_{ele}$), and hydrophobic energy ($\Delta E_{lipo}$) of mTAAR1-EPPTB system (-50.7, -11.1, and -44.9 kcal/mol) are respectively more negative than that of the hTAAR1-EPPTB system (-45.8, -8.1 and -42.6 kcal/mol), so that the averaged MM-GBSA binding energy ($\Delta G_{bind}$) value of mTAAR1-EPPTB (-106.7 kcal/mol) is more negative than that of hTAAR1-EPPTB (-96.5 kcal/mol), indicating that the EPPTB binding affinity to mTAAR1 is stronger than to hTAAR1. Moreover, in all MD trajectories, $\Delta E_{vdw}$ and $\Delta E_{lipo}$ make dominant contributions to the $\Delta G_{bind}$, while the $\Delta E_{ele}$ has a subtle contribution to the $\Delta G_{bind}$. It suggests that the packing interactions, contributed by van der Waals energy and hydrophobic energy, play an essential role for EPPTB binding to both mTAAR1 and hTAAR1.

**Table 1:** MM-GBSA binding energies ($\Delta G$, kcal/mol) of EPPTB bound to mTAAR1 and hTAAR1 during the last 100 ns MD simulations of three independent simulation trajectories.

| MM-GBSA | mTAAR1-EPPTB | | | | hTAAR1-EPPTB | | | |
|---|---|---|---|---|---|---|---|---|
| | **Traj 1** | **Traj 2** | **Traj 3** | **Average** | **Traj 1** | **Traj 2** | **Traj 3** | **Average** |
| $^1\Delta G_{bind}$ | -103.5±6.0 | -113.9 ± 6.6 | -102.6±9.5 | **-106.7±7.4** | -83.6 ±7 .7 | -104.4 ± 5.2 | -101.4±5.3 | **-96.5±6.1** |
| $^2\Delta E_{vdw}$ | -47.7 ± 3.0 | -53.9 ± 3.3 | -50.4±4.2 | **-50.7±3.5** | -40.8 ± 2.9 | -48.1± 2.1 | -48.6±2.4 | **-45.8±2.5** |
| $^3\Delta E_{ele}$ | -13.1± 2.4 | -10.0 ± 4.3 | -10.3±4.2 | **-11.1±3.6** | -5.0± 2.9 | -9.7 ± 2.7 | -9.6±2.7 | **-8.1±2.8** |

| | | | | | | | | |
|---|---|---|---|---|---|---|---|---|
| [4]$\Delta E_{lipo}$ | -42.7 ± 3.6 | -50.1 ± 2.2 | -41.8±3.8 | **-44.9±3.2** | -37.8 ± 3.0 | -46.7 ± 2.5 | -43.2±2.8 | **-42.6±2.8** |
| [5]$K_i$ (μM) | 0.0009 | | | | > 5 | | | |
| [6]$K_i$ (nM) | 0.9 ± 0.1 | | | | nd | | | |

[1]$\Delta G_{bind}$: MM-GBSA binding energy ($\Delta G_{bind} = \Delta G_{Complex} - \Delta G_{Receptor} - \Delta G_{Ligand}$).

[2]$\Delta E_{vdw}$: Change of van der Waals energy (Van der Waals + π-π stacking + Self-contact) in gas phase upon complex formation.

[3]$\Delta E_{ele}$: Change of electrostatic interactions (GB electrostatic solvation energy + Coulomb energy + Hydrogen-bond) upon complex formation.

[4]$\Delta E_{lipo}$: Change of lipophilic term (hydrophobic energy) upon complex formation.

[5]Experimental $K_i$ binding affinity (inhibitory constant) values obtained from [20, 21].

[6]$K_i$ binding affinity to HEK293 using the Radioligand [3H]-rac-2-(1,2,3,4-tetrahydro-1-naphthyl)-2-imidazoline Ref. [20].

**Ligand-receptor interaction data showed that hydrophobic interaction was the predominant interaction, but some key residues of m/hTAAR1 are different, which may be the original reason for weak binding affinity of hTAAR1 to EPPTB.**

The ligand-protein interactions for the mTAAR1 and hTAAR1 systems during total ~3.00 μs MD simulations were calculated using the SID tool. Specifically, the interaction diagrams lasting more than 10% MD simulation time and the interaction histograms along with interaction fraction for each type of interaction are shown in Fig. 2. The 2D-interaction diagrams show that the EPPTB was bond at the orthosteric binding sites of m/hTARR1. For mTAAR1 system, the ethoxyphenyl group of EPPTB is exposed to the solvent and the rest part (pyrrolidinyl-phenyl group) forms hydrophobic interactions with nearby residues, especially with $I103^{3.33}$, $I110^{3.40}$, $W261^{6.48}$, $F264^{6.51}$ and $A193^{5.42}$. EPPTB also forms water-mediated hydrogen bond with $D102^{3.32}$, hydrogen bonds with $Y153^{4.56}$ and $S189^{5.38}$, and π-π interaction with $F264^{6.51}$. As for hTAAR1 system, the whole EPPTB is exposed in the solvent and the pyrrolidinyl-phenyl group forms hydrophobic interactions with $I104^{3.33}$, $F195^{5.43}$, $F199^{5.47}$, $W264^{6.48}$ and $F267^{6.51}$. EPPTB also forms water-mediated hydrogen bonds with $D103^{3.32}$and $S107^{3.36}$, hydrogen bond with $V184^{ECL2}$, π-cation interaction with $R83^{2.64}$, π-π interactions with $F195^{5.43}$ and $W264^{6.48}$. Therefore, the hydrophobic interactions (including π-π interactions) are the predominant interactions between EPPTB and m/hTAAR1, which is accordance with the result of MM-GBSA calculations showing that packing interactions, contributed by van der Waals energy and hydrophobic energy, play an essential role for

EPPTB binding.

For both mTAAR1 system and hTAAR1 system, four common interaction residues of mTAAR1 and hTAAR1 were observed: D102$^{3.32}$ (of mTAAR1) / D103$^{3.32}$ (of hTAAR1), I103$^{3.33}$ / I104$^{3.33}$, W261$^{6.48}$ / W264$^{6.48}$, and F264$^{6.51}$ / F267$^{6.51}$. EPPTB not only could form water-mediated hydrogen bond with D102$^{3.32}$ for mTAAR1 and D103$^{3.32}$ for hTAAR1, but also could form hydrophobic interactions with I103$^{3.33}$, W261$^{6.48}$ and F264$^{6.51}$ for mTAAR1, and I104$^{3.33}$, W264$^{6.48}$ and F267$^{6.51}$ for hTAAR1.

However, some interaction residues of mTAAR1 and hTAAR1 are different. The interaction histograms of Fig. 2 show that EPPTB readily interacts with 7 residues (I110$^{3.40}$, Y153$^{4.56}$, F184$^{ECL2}$, S189$^{5.38}$, A193$^{5.42}$, T268$^{6.55}$ and Y287$^{7.39}$) of mTAAR1, but rarely interacts with the corresponding residues (I111$^{3.40}$, F154$^{4.56}$, F185$^{ECL2}$, S190$^{5.38}$, T194$^{5.42}$, T271$^{6.55}$ and I290$^{7.39}$) of hTAAR1. This could cause the binding affinity of EPPTB to hTAAR1 to be weaker than EPPTB to mTAAR1. When compared with the corresponding residues of hTAAR1, EPPTB has much stronger hydrophobic interactions with 4 out of the 7 residues of mTAAR1 (I110$^{3.40}$, F184$^{ECL2}$, A193$^{5.42}$, and Y287$^{7.39}$), and has much stronger hydrogen bond interactions with the rest of them (Y153$^{4.56}$, S189$^{5.38}$, and T268$^{6.55}$).

Especially, it is interesting to find that the three residues Y153$^{4.56}$, A193$^{5.42}$ and Y287$^{7.39}$ of mTAAR1 could interact with EPPTB with interactions fraction more than ~0.1, while the corresponding residues F154$^{4.56}$, T194$^{5.42}$ and I290$^{7.39}$ of hTAAR1 at the same position almost lost the interaction with EPPTB (Fig. 2 and Fig. S10). It indicates that the three amino acids at those positions could directly affect the binding affinity to EPPTB, and the three residues (Y153$^{4.56}$, A193$^{5.42}$ and Y287$^{7.39}$) may be the key residues of mTAAR1. The three residues (F154$^{4.56}$, T194$^{5.42}$ and I290$^{7.39}$) of hTAAR1 are different from the three corresponding residues (Y153$^{4.56}$, A193$^{5.42}$ and Y287$^{7.39}$) of mTAAR1, which would ultimately affect the binding between hTAAR1 and EPPTB.

On the contrary, EPPTB readily interacts with **6** residues (R83$^{2.64}$, S107$^{3.36}$, V184$^{ECL2}$, F186$^{ECL2}$, F195$^{5.43}$ and F199$^{5.47}$) of hTAAR1, but rarely interacts with the corresponding residues (R82$^{2.46}$, S106$^{3.36}$, P183$^{ECL2}$,

F185$^{ECL2}$, F194$^{5.43}$ and F198$^{5.47}$) of mTAAR1. This could cause the binding affinity of EPPTB to hTAAR1 to be stronger than EPPTB to mTAAR1. When compared with the corresponding residues of mTAAR1, EPPTB has much stronger hydrophobic interactions with **4** out of the **6** residues of mTAAR1 (R83$^{2.64}$, F186$^{ECL2}$, F195$^{5.43}$ and F199$^{5.47}$), and has much stronger hydrogen bond interactions with the rest residue of them (S107$^{3.36}$ and V184$^{ECL2}$).

Overall, the binding affinity contributed from the favorable residues of hTARR1 (R83$^{2.64}$, S107$^{3.36}$, V184$^{ECL2}$, F186$^{ECL2}$, F195$^{5.43}$ and F199$^{5.47}$) may be smaller than that of mTARR1 (I110$^{3.40}$, Y153$^{4.56}$, F184$^{ECL2}$, S189$^{5.38}$, A193$^{5.42}$, T268$^{6.55}$ and Y287$^{7.39}$), as a result, the total binding affinity of EPPTB to hTAAR1 would be weaker than that of EPPTB to mTAAR1. Especially, the several residues in binding site of hTAAR1 (F154$^{4.56}$, T194$^{5.42}$ and I290$^{7.39}$) are different from these of mTAAR1 (Y153$^{4.56}$, A193$^{5.42}$ and Y287$^{7.39}$), which may be the original and essential factor that cause hTAAR1 to have lower binding affinity to EPPTB. This speculation is reasonable and agreement with the result of MM-GBSA calculation.

In addition, the protein-ligand interactions of the two systems during the three independent ~1.0 μs MD simulations (Trajectory **1,** Trajectory **2,** and Trajectory **3**) are also shown in Figs. S11-S12, which also showed that the hydrophobic interactions play an essential role for EPPTB binding to m/hTARR1.

The hTAAR1's thirteen residues proposed by Cichero *et al.* were seemed to interact with EPPTB during their simulation. Out of the thirteen residues, eleven residues appeared in our simulations of hTAAR1-EPPTB system; night residues appeared in our simulations of mTAAR1-EPPTB system (Table S2)[18]. It means that our binding site of m/hTAAR1 is the same as that of the earlier study, which further confirms the credibility of our calculation results.

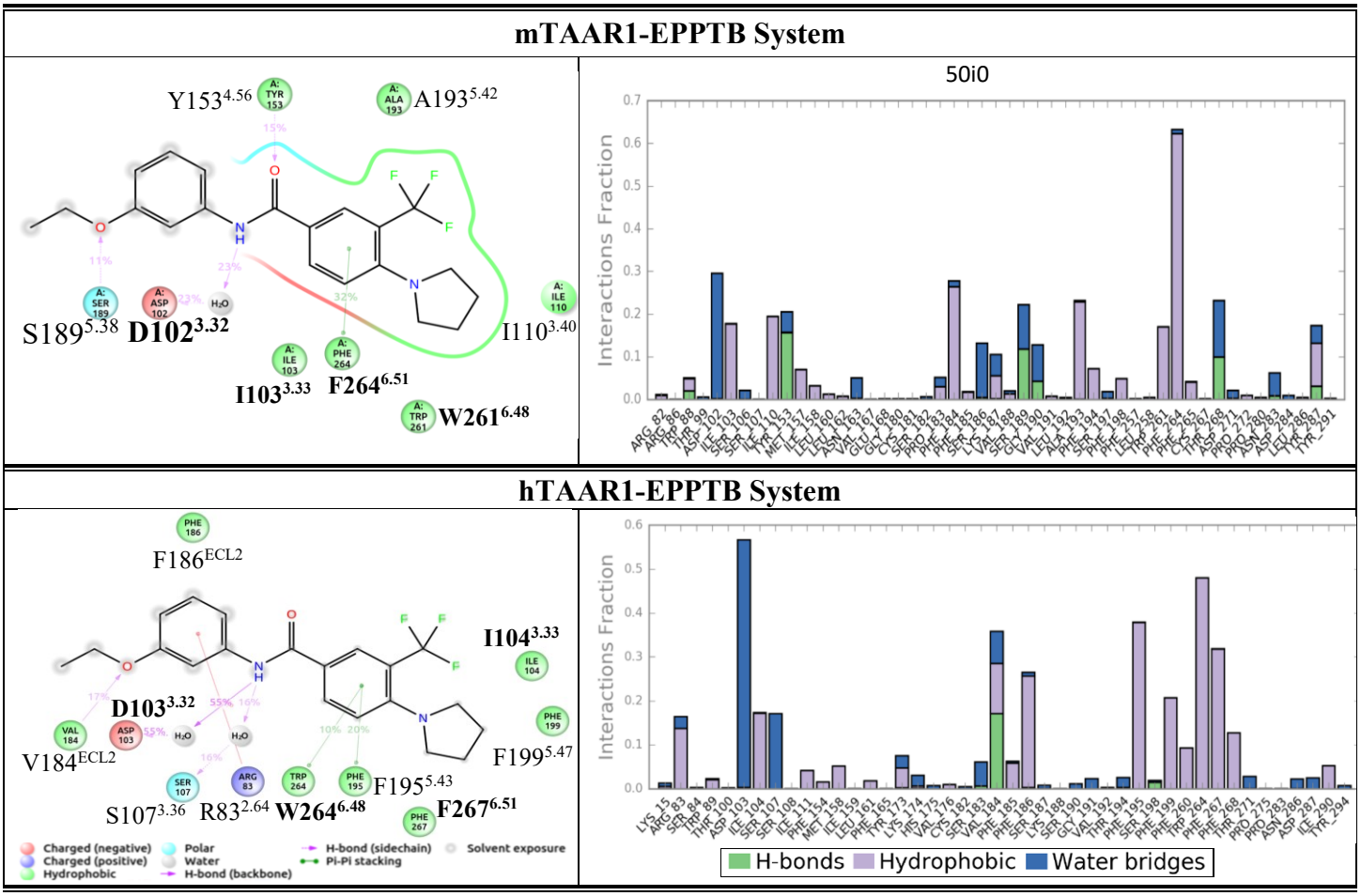


**Fig. 2.** The 2D-interaction diagrams (left) and interaction histograms (right) of the mTAAR1-EPPTB and hTAAR1-EPPTB systems during ~3.0 μs MD simulations. The Protein-Ligand interactions lasting more than 10% MD simulation time are shown. All residues that interact with the ligand EPPTB are shown in the histogram along with the interactions fraction for each type of interaction.

**Clustering analysis showed the EPPTB exhibited diversified conformations, which could be used to screen novel compounds with higher binding affinity to mTAAR1 or hTAAR1 in the future.**

To identify the major binding poses for each system, we clustered the eight complex structures from the ~3.0 μs MD simulations and aligned them. The representative structures are in the top abundant clusters (>4.5%) are shown in Fig. S13. The two simulation systems both showed to have numerous clusters. Within the mTAAR1-EPPTB system, the top eight clusters have the percentages of 12.0%, 9.4%, 9.1%, 9.1%, 8.5%, 8.1%, 7.0%, and 6.5% respectively, while within the hTAAR1-EPPTB system, the clusters have the percentages of 20.3%, 16.6%, 9.5%, 8.8%, 8.5%, 5.5%, 5.0%, and 4.7% respectively. The clustering of the EPPTB showed that all

conformations of EPPTB were located within the orthosteric binding site of m/hTARR1 (Fig. S16A). Most of the binding poses of EPPTB were vertically located into the binding site, with ethoxyphenyl group facing up to extracellular section and the pyrrolidinyl group facing down to the central position within the 7TMs bundle. Moreover, the 2D-interaction diagrams for the representative structures (without water molecules) of the top **8** structural clusters are also shown in Fig S16B. It also showed that the hydrophobic interactions play a predominant role for EPPTB binding to m/hTARR1. Although the **8** binding poses of EPPTB in each system showed differences in orientation, but EPPTB still located in the orthosteric binding site of m/hTARR1.

Unfortunately, since there have been no experimental reports on the conformation of TAAR1 so far, we are not able to compare our results with the related experimental data. Overall, the clustering results showed that the two systems exhibited multiple conformations during the MD simulations. There are **8** different confirmations for m/h TAAR1 when interacting with EPPTB. All possible receptor conformations that interact with ligands should be considered, in order to obtain more potential novel compounds. Therefore, these **8** representative conformations could be used to screen new compounds with higher binding affinity to mTAAR1 or hTAAR1 in the future.

In addition, the superimposition of each representative structure in the most abundant cluster for mTAAR1-EPPTB complex (12.0%) and hTAAR1-EPPTB complex (20.3%) is shown in Fig. 3, which clearly illustrates the differences in ligand-protein contacts. The two binding poses of EPPTB showed differences in orientation, and EPPTB in mTAAR1 was shown to be closer to TM3-5 than it in hTAAR1. Meanwhile, as for the conformations of mTAAR1 and hTAAR1, except for the conformational differences in the extracellular end of the TM1 possibly due to the terminal effect of the N-terminal, the two ends of TM5, intracellular end of TM6, extracellular loop (ECL) 2 and intracellular loop (ICL) 3 were also shown to be greatly different. These differences in protein conformation will inevitably lead to the difference in the binding affinity of m/hTAAR1 to EPPTB.

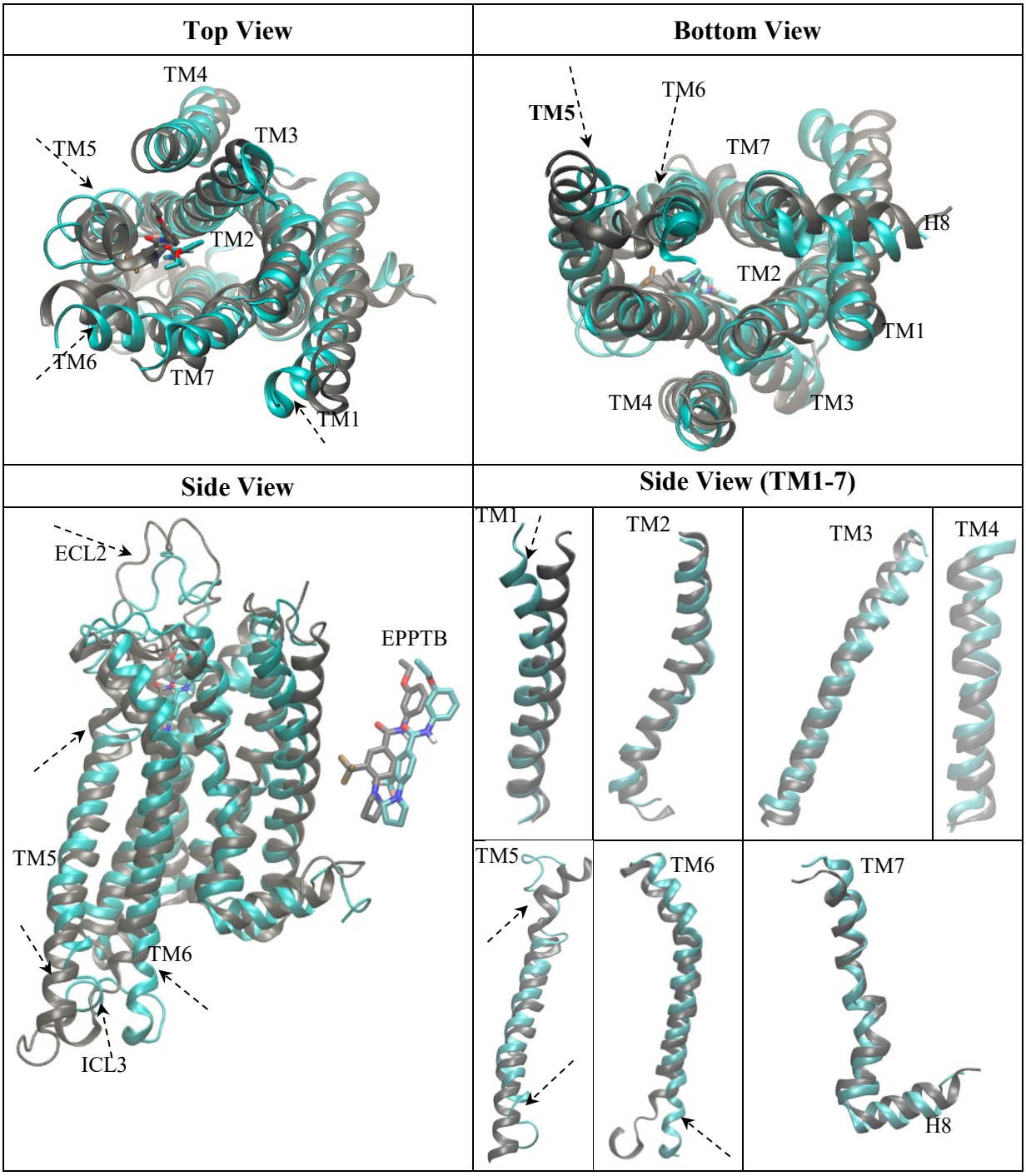


**Fig. 3.** The representative structures of the most abundant clusters for the mTAAR1-EPPTB complex (gray) and hTAAR1-EPPTB complex (cyan) are superimposed for comparison from different views. The receptors are represented by ribbon and the ligands are represented by sticks with the same color as its corresponding receptor. For clarity, some intracellular and extracellular loops were omitted and the differences in TMs are marked by arrows.

**The protein Secondary Structure Element (SSE) analyses also identified that the differences in TM5-6 helices of the two receptors.**

In order to investigate the differences on the secondary structure of the receptor, the protein SSE analysis in Fig. 5 for the two systems throughout the simulations were also performed using the SID tool. Noticeable changes in helical structures of hTAAR1 are observed primarily at the left end of TM1, two ends of TM5 and ICL3, showing smaller SSE values indicating a loss of helical structures with the increase of coil structures. It is consistent with the above clustering result that the two ends of TM5 of hTAAR1 displayed coil structures (Fig. 4). Moreover, these SSE percentage changes of secondary structure must cause relevant changes in the corresponding TMs in the 3D structure, which could explain why the conformation differences were shown at the TM1, TM5-6, and ICL3 (Fig. 4). Additionally, the beta sheets in ECL2 of the mTAAR1 and hTAAR1 are extremely negligible, indicating that these beta sheets are extremely unstable and are prone to transform into coil structures, so that the ECL2 sections of the two proteins will fluctuate violently during the MD simulations.

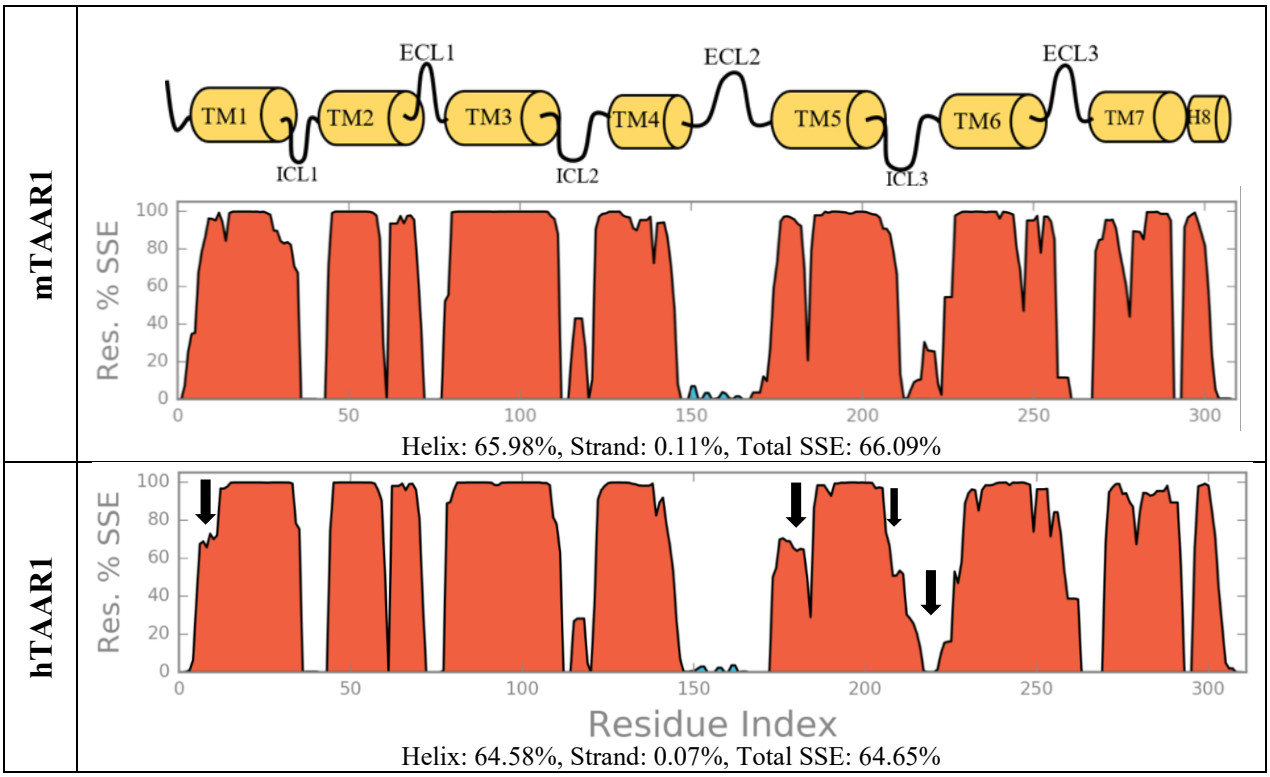


**Fig. 4.** Protein Secondary Structure Element (SSE) distributions by residues for mTAAR1 and hTAAR1 during ~3.0 μs MD simulations are shown, where the α-helices are represented in red, and the β-strands are represented

in blue. In addition, the above TAAR1 architecture is for reference, and the arrows show the structural difference between the mTAAR1 and hTAAR1.

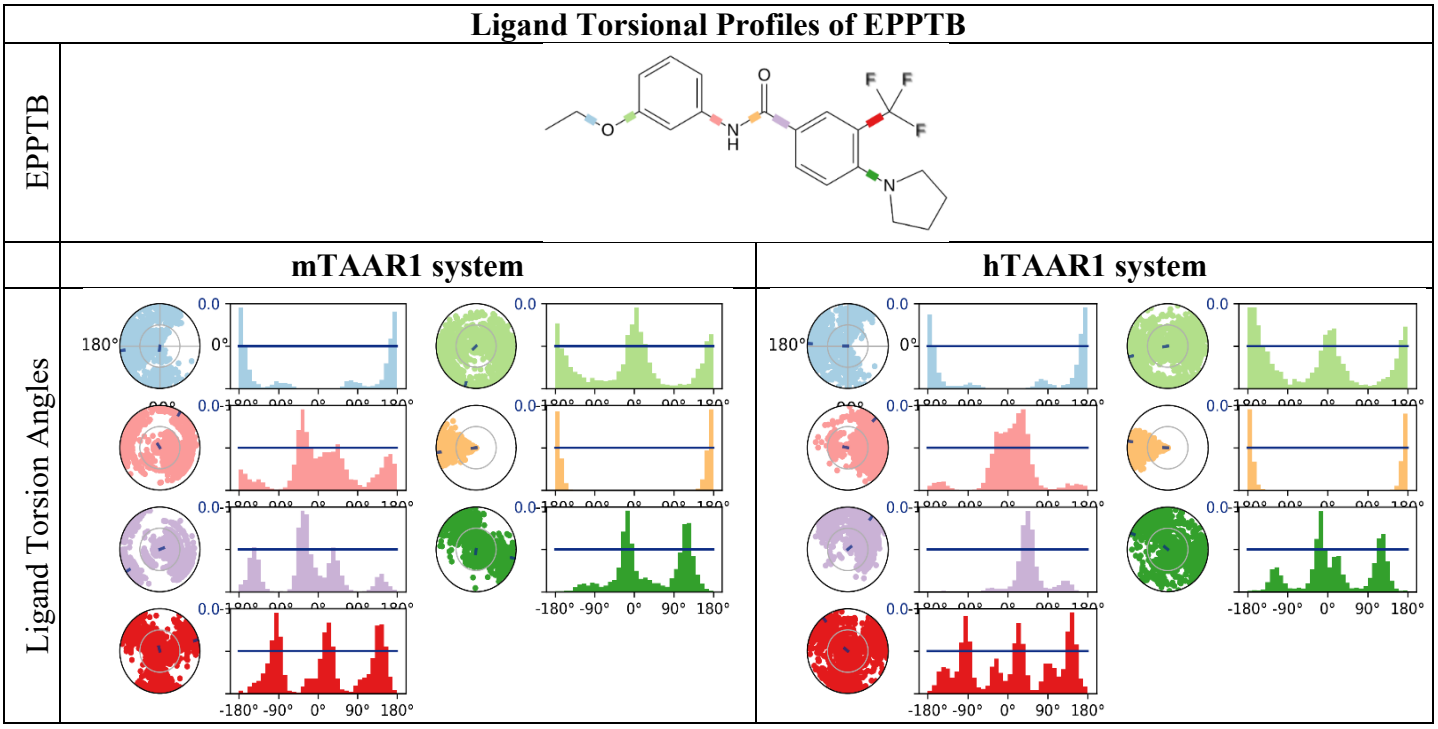


**Fig. 5.** The ligand torsional profiles being the conformational progression of the seven rotatable bonds of EPPTB during ~3.0 μs MD simulations (0 through 1,000 ns) are shown. The dial plots describe the conformation of the torsion throughout the course of the simulation. The beginning of the simulation is in the center of the radial plot and the time evolution is plotted radially outwards. The bar plots summarize the data on the dial plots, by showing the probability density of the torsion. In addition, the 2D structure of EPPTB in top panel is for reference.

**Ligand Torsional Profiles indicates that improving the stability of the pyrrolidinyl group of EPPTB might enhance the binding affinity to hTAAR1.**

The ligand torsional profiles (Fig. 5) summarized the conformational evolution of every rotatable bond in the EPPTB throughout the simulation trajectories (0.00 through 1,000 ns). For both systems, three rotatable bonds of the EPPTB in light blue, light green and yellow respectively have similar distributions, meaning that these bonds have similar rotational confirmations during the MD simulations. However, compared with the mTAAR1-EPPTB system, the pink- and purple-colored rotational bonds of EPPTB show a narrower distribution in the bar plots of the hTAAR1-EPPTB system. While the dial plots of the hTAAR1-EPPTB system, the green and red colored rotational bonds of EPPTB shows a wider distribution. This indicates that the pyrrolidinyl and

trifluoromethyl groups of EPPTB are more fluctuant in the hTAAR1-EPPTB system. Therefore, modifying the pyrrolidinyl group of EPPTB to improve its stability may be an ideal way to enhance the binding affinity of EPPTB to hTAAR1.

**Discussion**

The compound EPPTB is a highly selective antagonist of mTAAR1 but not for hTAAR1[20], which considerably impedes the progresses in exploiting the properties of EPPTB for mental illness treatment and studying the basic biological functions of hTAAR1. Discovering new lead compounds with high binding affinity to hTAAR1 are in critical need. Since there are not any available high-resolution crystal structures of TAAR1, we use these calculation methods of the homology modeling, molecular docking, and MD simulations to probe detailed structural and dynamic insights of interactions between EPPTB and m/hTARR1, and to present potential EPPTB-bound hTARR1 conformations for screening its new compounds with high binding affinity to hTAAR1.

The RMSD values show that it took longer time for EPPTB in mTAAR1 to reach stead state than than it did in hTAAR1, but EPPTB in hTAAR1 appears to be fluctuated more than mTAAR1 during the MD simulations (Fig. 1). The noticeable decrease of SSE values for hTAAR1 is observed primarily at the left end of TM1, the ends of TM5-6 and ICL3; the beta sheets in ECL2 are extremely negligible (Fig. 4). These suggest that these positions may have larger conformational changes, which is consistent with the differences in the top representative structures of the m/h TAAR1 are at the TM1, TM5-6, ECL2 and ICL3 (Fig. 3). These differences in ligand fluctuation and receptor conformations during the MD simulation will inevitably contribute to the difference in the binding affinity of m/hTAAR1 to EPPTB.

Both the XP docking score and averaged MM-GBSA binding energy ($\Delta G_{bind}$) of mTAAR1-EPPTB complex (-10.21 and -106.7 kcal/mol, respectively) are more negative than that of hTAAR1-EPPTB complex (-8.16 and -96.5 kcal/mol respectively). These calculated results consistently support the experimental result that the EPPTB binding affinity of mTAAR1 ($K_i$ =0.0009 μM) is stronger than that of hTAAR1 ($K_i$ > 5 μM)[21]. Additional

binding affinity for the interaction of EPPTB and the TAAR1 was verified experimentally using a radioligand with HEK293, which found that the $K_i$ value for the mTAAR1 was 0.9 ± 0.1 nM, while for the hTAAR1 was undetectable[20].

The sequence identity of the mTAAR1 and hTAAR1 is ~74.0% similarity to one another, and some key residues in the orthosteric binding sites of the two proteins are different. In the protein-ligand interactions, EPPTB is prone to only interact with the **7** residues (I110$^{3.40}$, Y153$^{4.56}$, F184$^{ECL2}$, S189$^{5.38}$, A193$^{5.42}$, T268$^{6.55}$ and Y287$^{7.39}$) of mTAAR1, but EPPTB is prone to only interact with the **6** residues (R83$^{2.64}$, S107$^{3.36}$, V184$^{ECL2}$, F186$^{ECL2}$, F195$^{5.43}$ and F199$^{5.47}$) of hTAAR1 (Fig. 2). Overall, the binding affinity contributed from the **6** favorable residues of hTARR1 may be smaller than the binding affinity contributed from the **7** favorable residues of mTARR1, as a result, the total binding affinity of EPPTB to hTAAR1 would be weaker than that of EPPTB to mTAAR1. Especially, among these **13** residues of m/h TAAR1, the three residues Y153$^{4.56}$, A193$^{5.42}$ and Y287$^{7.39}$ of mTAAR1 can interact with EPPTB well, while the corresponding residues F154$^{4.56}$, T194$^{5.42}$ and I290$^{7.39}$ of hTAAR1 at the same position are different amino acids and they almost lost the interaction with EPPTB. Therefore, the three residues (Y153$^{4.56}$, A193$^{5.42}$ and Y287$^{7.39}$) may be the key residues of mTAAR1; the several residues in binding site of hTAAR1 (F154$^{4.56}$, T194$^{5.42}$ and I290$^{7.39}$) are different from these of mTAAR1 (Y153$^{4.56}$, A193$^{5.42}$ and Y287$^{7.39}$), which may be the original reason that cause hTAAR1 to have lower binding affinity to EPPTB. This speculation is reasonable and agreement with the results of a previous study investigated by Tan *et. al*[57]. They found that each site-directed mutation of Y153$^{4.56}$F, T268$^{6.55}$M, and Y287$^{7.39}$N of mouse TAAR1, and A193$^{5.42}$T of rat TAAR1, could affect the agonist selectivity of rat (r) and mouse TAAR1. The experimental result also verified that these residues Y153$^{4.56}$, A193$^{5.42}$, T268$^{6.55}$, and Y287$^{7.39}$ of mTAAR1 were the key residues of mTAAR1. The good agreement between our result and the previous one further confirms the credibility of our calculation results.

The Van der Waals energy ($\Delta E_{vdw}$) and hydrophobic energy ($\Delta E_{lipo}$) make dominant contributions to the binding energy ($\Delta G_{bind}$), indicating that the packing interactions, contributed by van der Waals energy and hydrophobic energy, play an essential role for EPPTB binding to both m/hTAAR1 (Table 1). On the other hand, the binding modes of the two complexes show that the pyrrolidinyl phenyl group of EPPTB primarily forms the hydrophobic interactions with residues nearby, especially with especially $I103^{3.33}$, $W261^{6.48}$ and $F264^{6.51}$ for the mTAAR1, and $I104^{3.33}$, $W264^{6.48}$ and $F267^{6.51}$ for the hTAAR1. The importance of the aromatic residues ($W261^{6.48}$, $F264^{6.51}$ for mTAAR1, and $W264^{6.48}$, $F267^{6.51}$ for hTAAR1) of aminergic receptors has been identified by site-directed mutagenesis, and they interact with aromatic moiety of ligand through hydrophobic interactions[58-60]. Therefore, it is credible that the hydrophobic interactions (including π-π interactions) are the essential interactions for EPPTB binding to m/hTARR1.

Moreover, most residues in the putative binding site of our EPPTB-hTAAR1 simulation system are consistent with the residues proposed by Cichero *et al*[18] in modeling EPPTB-hTAAR1( Table S2) . In the putative binding site, four common interaction residues of mTAAR1 and hTAAR1 were observed: $D102^{3.32}$ (of mTAAR1) / $D103^{3.32}$ (of hTAAR1), $I103^{3.33}$ / $I104^{3.33}$, $W261^{6.48}$ / $W264^{6.48}$, and $F264^{6.51}$ / $F267^{6.51}$. EPPTB not only could form the hydrophobic interactions, but also could form water-mediated hydrogen bond with $D102^{3.32}$ for mTAAR1 and $D103^{3.32}$ for hTAAR1. The importance of the conserved residue ($D102^{3.32}$ / $D103^{3.32}$) of aminergic receptors has been identified by site-directed mutagenesis, and it forms a hydrogen bond with the cationic amine of the ligand[59, 60].

Using a homology model of hTAAR1, It is inspiring that Cichero et al. [18] have identified an novel hTAAR1 antagonist Compound **3** with IC50=9.0 μM. To see if this compound binds differently to our homology models of mTAAR1 and hTAAR1, induced fit dockings to these two homology models were carried out and the binding poses are shown in Figure S18. Indeed, its binding poses to mTAAR1 is different from its binding poses to hTAAR1. While the binding poses to hTAAR1 are clustered tightly in one cluster, the poses to mTAAR1 are distributed widely in several clusters. The best binding pose for mTAAR1 and hTAAR1 was picked for further

comparison (Figure S19): 1). Compound **3** binds to different pockets of the two receptors. 2). Its XP docking score to hTAAR1 (-9.91 kcal/mol) is slightly better that to mTAAR1 (-9.23 kcal/mol), suggesting a binding preference to hTAAR1. When comparing the binding of compound **3** to hTAAR1 with the binding of EPPTB to hTAAR1, 1). Interestingly, both antagonists bind to a very similar pocket (Figure S18 VS Figure S6). 2). The XP docking score of compound **3** (-9.91 kcal/mol) is slightly worse than EPPTB (-10.21 kcal/mol), this order is consistent with the experimental order (IC50=9.0 μM of Compound **3** vs Ki=0.9 nM of EPPTB) despite the magnitude of the difference is much smaller than the experimental difference.

The ligand torsional profiles show that the pyrrolidinyl group of EPPTB are more fluctuant in hTAAR1-EPPTB system, indicating that modifying the group to improve its stability might be able to enhance the binding affinity of EPPTB to hTAAR1. Moreover, there are **8** different confirmations for m/h TAAR1 that can be expressed when interacting with EPPTB. All possible receptor conformations that interact with ligands should be taken into account, in order to obtain more potential compounds. Therefore, the **8** representative conformations could be used to screen novel antagonists with higher binding affinity to mTAAR1 or hTAAR1 in near future.

**Conclusion**

This study uses the homology modeling, molecular docking, and MD simulations to investigate binding poses of EPPTB in both mTAAR1 and hTAAR1 and identify key binding interactions in the binding site. The MM-GBSA binding energies and XP docking scores showed that the EPPTB exhibited stronger binding affinity to mTAAR1 than it did to hTAAR1, which was consistent with the previous experimental result. The hydrophobic interactions played an essential role in the binding of EPPTB to m/hTAAR1. EPPTB not only could form water-mediated hydrogen bond with $D102^{3.32}$ for mTAAR1 and $D103^{3.32}$ for hTAAR1, but also could form hydrophobic interactions with $I103^{3.33}$, $W261^{6.48}$ and $F264^{6.51}$ for mTAAR1, and $I104^{3.33}$, $W264^{6.48}$ and $F267^{6.51}$ for hTAAR1. Additionally, EPPTB is prone to only interact with the **7** residues ($I110^{3.40}$, $Y153^{4.56}$, $F184^{ECL2}$,

S189$^{5.38}$, A193$^{5.42}$, T268$^{6.55}$ and Y287$^{7.39}$) of mTAAR1, but EPPTB is prone to only interact with the **6** residues (R83$^{2.64}$, S107$^{3.36}$, V184$^{ECL2}$, F186$^{ECL2}$, F195$^{5.43}$ and F199$^{5.47}$) of hTAAR1. Overall, the several residues in binding site of hTAAR1 (F154$^{4.56}$, T194$^{5.42}$ and I290$^{7.39}$) are different from these of mTAAR1 (Y153$^{4.56}$, A193$^{5.42}$ and Y287$^{7.39}$), which may be a critical factor that could cause hTAAR1 to have lower binding affinity to EPPTB. Furthermore, eight potential EPPTB-bound hTARR1 conformations were obtained from the clustering analysis on the MD trajectories and could be used to screen new antagonists with higher binding affinity to hTAAR1 in future. Our docking analysis on another hTAAR1 antagonist Compound **3** have found that 1). this compound binds in different pockets of our mTAAR1 and hTAAR1 homology models with a slightly stronger binding affinity to hTAAR1; 2). both antagonists bind to a very similar pocket of hTAAR1.

**Conflicts of interest**

All of the authors declare no conflicts of interest.

**Acknowledgements**

This work was supported by Rowan University CSM SEED fund and the National Science Foundation of USA under Grant RUI-1904797. We also acknowledge the High-Performance Computing Facility at Rowan funded by the National Science Foundation of USA under Grant MRI-1429467 and XSEDE MCB160164/160173/170088. The Anton2 machine at the Pittsburgh Supercomputing Center (PSCA17017P) was generously made available by D. E. Shaw Research.

## REFERENCES**Uncategorized References**


[1] B. Borowsky, N. Adham, K.A. Jones, R. Raddatz, R. Artymyshyn, K.L. Ogozalek, M.M. Durkin, P.P. Lakhlani, J.A. Bonini, S. Pathirana, N. Boyle, X. Pu, E. Kouranova, H. Lichtblau, F.Y. Ochoa, T.A. Branchek, C. Gerald, Trace amines: identification of a family of mammalian G protein-coupled receptors, Proc Natl Acad Sci U S A, 98 (2001) 8966-8971.
[2] J.R. Bunzow, M.S. Sonders, S. Arttamangkul, L.M. Harrison, G. Zhang, D.I. Quigley, T. Darland, K.L. Suchland, S. Pasumamula, J.L. Kennedy, S.B. Olson, R.E. Magenis, S.G. Amara, D.K. Grandy, Amphetamine, 3,4-methylenedioxymethamphetamine, lysergic acid diethylamide, and metabolites of the catecholamine neurotransmitters are agonists of a rat trace amine receptor, Mol Pharmacol, 60 (2001) 1181-1188.
[3] R. Zucchi, G. Chiellini, T.S. Scanlan, D.K. Grandy, Trace amine-associated receptors and their ligands, Br J Pharmacol, 149 (2006) 967-978.
[4] J.F. Liu, J.X. Li, TAAR1 in Addiction: Looking Beyond the Tip of the Iceberg, Front Pharmacol, 9 (2018) 279.
[5] F.G. Revel, J.L. Moreau, R.R. Gainetdinov, A. Bradaia, T.D. Sotnikova, R. Mory, S. Durkin, K.G. Zbinden, R. Norcross, C.A. Meyer, V. Metzler, S. Chaboz, L. Ozmen, G. Trube, B. Pouzet, B. Bettler, M.G. Caron, J.G. Wettstein, M.C. Hoener, TAAR1 activation modulates monoaminergic neurotransmission, preventing hyperdopaminergic and hypoglutamatergic activity, Proc Natl Acad Sci U S A, 108 (2011) 8485-8490.
[6] M.D. Berry, R.R. Gainetdinov, M.C. Hoener, M. Shahid, Pharmacology of human trace amine-associated receptors: Therapeutic opportunities and challenges, Pharmacol Ther, 180 (2017) 161-180.
[7] R.R. Gainetdinov, M.C. Hoener, M.D. Berry, Trace Amines and Their Receptors, Pharmacol Rev, 70 (2018) 549-620.
[8] D.K. Grandy, Trace amine-associated receptor 1-Family archetype or iconoclast?, Pharmacol Ther, 116 (2007) 355-390.
[9] G. Rutigliano, A. Accorroni, R. Zucchi, The Case for TAAR1 as a Modulator of Central Nervous System Function, Front Pharmacol, 8 (2017) 987.
[10] G. Chiellini, G. Nesi, M. Digiacomo, R. Malvasi, S. Espinoza, M. Sabatini, S. Frascarelli, A. Laurino, E. Cichero, M. Macchia, R.R. Gainetdinov, P. Fossa, L. Raimondi, R. Zucchi, S. Rapposelli, Design, Synthesis, and Evaluation of Thyronamine Analogues as Novel Potent Mouse Trace Amine Associated Receptor 1 (mTAAR1) Agonists, J Med Chem, 58 (2015) 5096-5107.
[11] G. Chiellini, G. Nesi, S. Sestito, S. Chiarugi, M. Runfola, S. Espinoza, M. Sabatini, L. Bellusci, A. Laurino, E. Cichero, R.R. Gainetdinov, P. Fossa, L. Raimondi, R. Zucchi, S. Rapposelli, Hit-to-Lead Optimization of Mouse Trace Amine Associated Receptor 1 (mTAAR1) Agonists with a Diphenylmethane-Scaffold: Design, Synthesis, and Biological Study, J Med Chem, 59 (2016) 9825-9836.
[12] M.R. Edelmann, T. Hartung, R. Trussardi, H. Iding, G. Galley, P. Pflieger, R.D. Norcross, Synthesis of enantiomerically pure [(14) C]-labelled morpholine derivatives for a class of trace amine-associate receptor 1 agonists, J Labelled Comp Radiopharm, 59 (2016) 635-639.
[13] G. Galley, A. Beurier, G. Decoret, A. Goergler, R. Hutter, S. Mohr, A. Pahler, P. Schmid, D. Turck, R. Unger, K.G. Zbinden, M.C. Hoener, R.D. Norcross, Discovery and Characterization of 2-Aminooxazolines as Highly Potent, Selective, and Orally Active TAAR1 Agonists, ACS Med Chem Lett, 7 (2016) 192-197.
[14] G. Galley, H. Stalder, A. Goergler, M.C. Hoener, R.D. Norcross, Optimisation of imidazole compounds as selective TAAR1 agonists: discovery of RO5073012, Bioorg Med Chem Lett, 22 (2012) 5244-5248.
[15] S. Guariento, M. Tonelli, S. Espinoza, A.S. Gerasimov, R.R. Gainetdinov, E. Cichero, Rational design, chemical synthesis and biological evaluation of novel biguanides exploring species-specificity responsiveness of TAAR1 agonists, Eur J Med Chem, 146 (2018) 171-184.
[16] M. Tonelli, S. Espinoza, R.R. Gainetdinov, E. Cichero, Novel biguanide-based derivatives scouted as TAAR1 agonists: Synthesis, biological evaluation, ADME prediction and molecular docking studies, Eur J Med Chem, 127 (2017) 781-792.
[17] P.C. Nair, J.O. Miners, R.A. McKinnon, C.J. Langmead, K.J. Gregory, D. Copolov, S.K.W. Chan, T. Bastiampillai, Binding of SEP-363856 within TAAR1 and the 5HT1A receptor: implications for the design of novel antipsychotic drugs, Mol Psychiatry, 27 (2022) 88-94.
[18] E. Cichero, S. Espinoza, S. Franchini, S. Guariento, L. Brasili, R.R. Gainetdinov, P. Fossa, Further insights into the pharmacology of the human trace amine-associated receptors: discovery of novel ligands for TAAR1 by a virtual screening approach, Chem Biol Drug Des, 84 (2014) 712-720.

[19] E. Cichero, S. Espinoza, R.R. Gainetdinov, L. Brasili, P. Fossa, Insights into the structure and pharmacology of the human trace amine-associated receptor 1 (hTAAR1): homology modelling and docking studies, Chem Biol Drug Des, 81 (2013) 509-516.
[20] A. Bradaia, G. Trube, H. Stalder, R.D. Norcross, L. Ozmen, J.G. Wettstein, A. Pinard, D. Buchy, M. Gassmann, M.C. Hoener, B. Bettler, The selective antagonist EPPTB reveals TAAR1-mediated regulatory mechanisms in dopaminergic neurons of the mesolimbic system, Proc Natl Acad Sci U S A, 106 (2009) 20081-20086.
[21] H. Stalder, M.C. Hoener, R.D. Norcross, Selective antagonists of mouse trace amine-associated receptor 1 (mTAAR1): discovery of EPPTB (RO5212773), Bioorg Med Chem Lett, 21 (2011) 1227-1231.
[22] K. Zhu, T. Day, D. Warshaviak, C. Murrett, R. Friesner, D. Pearlman, Antibody structure determination using a combination of homology modeling, energy-based refinement, and loop prediction, Proteins, 82 (2014) 1646-1655.
[23] T. Hou, J. Wang, Y. Li, W. Wang, Assessing the performance of the molecular mechanics/Poisson Boltzmann surface area and molecular mechanics/generalized Born surface area methods. II. The accuracy of ranking poses generated from docking, J Comput Chem, 32 (2011) 866-877.
[24] D.A. Goldfeld, K. Zhu, T. Beuming, R.A. Friesner, Successful prediction of the intra- and extracellular loops of four G-protein-coupled receptors, Proc Natl Acad Sci U S A, 108 (2011) 8275-8280.
[25] J. Li, R. Abel, K. Zhu, Y. Cao, S. Zhao, R.A. Friesner, The VSGB 2.0 model: a next generation energy model for high resolution protein structure modeling, Proteins, 79 (2011) 2794-2812.
[26] V. Kumar Bhardwaj, R. Purohit, S. Kumar, Himalayan bioactive molecules as potential entry inhibitors for the human immunodeficiency virus, Food Chem, 347 (2021) 128932.
[27] J. Sharma, V.K. Bhardwaj, P. Das, R. Purohit, Identification of naturally originated molecules as gamma-aminobutyric acid receptor antagonist, J Biomol Struct Dyn, 39 (2021) 911-922.
[28] R. Singh, V. Bhardwaj, R. Purohit, Identification of a novel binding mechanism of Quinoline based molecules with lactate dehydrogenase of Plasmodium falciparum, J Biomol Struct Dyn, 39 (2021) 348-356.
[29] R. Singh, V.K. Bhardwaj, R. Purohit, Potential of turmeric-derived compounds against RNA-dependent RNA polymerase of SARS-CoV-2: An in-silico approach, Comput Biol Med, 139 (2021) 104965.
[30] R. Singh, V.K. Bhardwaj, J. Sharma, P. Das, R. Purohit, Identification of selective cyclin-dependent kinase 2 inhibitor from the library of pyrrolone-fused benzosuberene compounds: an in silico exploration, J Biomol Struct Dyn, (2021) 1-9.
[31] R. Singh, V.K. Bhardwaj, J. Sharma, P. Das, R. Purohit, Discovery and in silico evaluation of aminoarylbenzosuberene molecules as novel checkpoint kinase 1 inhibitor determinants, Genomics, 113 (2021) 707-715.
[32] R. Singh, V.K. Bhardwaj, J. Sharma, R. Purohit, Identification of novel and selective agonists for ABA receptor PYL3, Plant Physiol Biochem, 154 (2020) 387-395.
[33] E. Harder, W. Damm, J. Maple, C. Wu, M. Reboul, J.Y. Xiang, L. Wang, D. Lupyan, M.K. Dahlgren, J.L. Knight, J.W. Kaus, D.S. Cerutti, G. Krilov, W.L. Jorgensen, R. Abel, R.A. Friesner, OPLS3: A Force Field Providing Broad Coverage of Drug-like Small Molecules and Proteins, J Chem Theory Comput, 12 (2016) 281-296.
[34] G.M. Sastry, M. Adzhigirey, T. Day, R. Annabhimoju, W. Sherman, Protein and ligand preparation: parameters, protocols, and influence on virtual screening enrichments, J Comput Aided Mol Des, 27 (2013) 221-234.
[35] M. Magrane, C. UniProt, UniProt Knowledgebase: a hub of integrated protein data, Database (Oxford), 2011 (2011) bar009.
[36] R.A. Friesner, J.L. Banks, R.B. Murphy, T.A. Halgren, J.J. Klicic, D.T. Mainz, M.P. Repasky, E.H. Knoll, M. Shelley, J.K. Perry, D.E. Shaw, P. Francis, P.S. Shenkin, Glide: a new approach for rapid, accurate docking and scoring. 1. Method and assessment of docking accuracy, J Med Chem, 47 (2004) 1739-1749.
[37] R.A. Friesner, R.B. Murphy, M.P. Repasky, L.L. Frye, J.R. Greenwood, T.A. Halgren, P.C. Sanschagrin, D.T. Mainz, Extra precision glide: docking and scoring incorporating a model of hydrophobic enclosure for protein-ligand complexes, J Med Chem, 49 (2006) 6177-6196.
[38] P. Jha, S. Chaturvedi, R. Bhat, N. Jain, A.K. Mishra, Insights of ligand binding in modeled h5-HT1A receptor: homology modeling, docking, MM-GBSA, screening and molecular dynamics, J Biomol Struct Dyn, (2021) 1-13.
[39] T. Lei, Z. Hu, R. Ding, J. Chen, S. Li, F. Zhang, X. Pu, N. Zhao, Exploring the Activation Mechanism of a Metabotropic Glutamate Receptor Homodimer via Molecular Dynamics Simulation, ACS Chem Neurosci, 11 (2020) 133-145.

[40] W.L. Jorgensen, D.S. Maxwell, J. Tirado-Rives, Development and Testing of the OPLS All-Atom Force Field on Conformational Energetics and Properties of Organic Liquids, Journal of the American Chemical Society, 118 (1996) 11225-11236.
[41] D. Shivakumar, J. Williams, Y. Wu, W. Damm, J. Shelley, W. Sherman, Prediction of Absolute Solvation Free Energies using Molecular Dynamics Free Energy Perturbation and the OPLS Force Field, J Chem Theory Comput, 6 (2010) 1509-1519.
[42] E. Lyman, C. Higgs, B. Kim, D. Lupyan, J.C. Shelley, R. Farid, G.A. Voth, A role for a specific cholesterol interaction in stabilizing the Apo configuration of the human A(2A) adenosine receptor, Structure, 17 (2009) 1660-1668.
[43] P. Mark, L. Nilsson, Structure and Dynamics of the TIP3P, SPC, and SPC/E Water Models at 298 K, The Journal of Physical Chemistry A, 105 (2001) 9954-9960.
[44] J.P. Jambeck, A.P. Lyubartsev, An Extension and Further Validation of an All-Atomistic Force Field for Biological Membranes, J Chem Theory Comput, 8 (2012) 2938-2948.
[45] J.B. Klauda, R.M. Venable, J.A. Freites, J.W. O'Connor, D.J. Tobias, C. Mondragon-Ramirez, I. Vorobyov, A.D. MacKerell, R.W. Pastor, Update of the CHARMM All-Atom Additive Force Field for Lipids: Validation on Six Lipid Types, Journal of Physical Chemistry B, 114 (2010) 7830-7843.
[46] D. Wang, H. Yu, X. Liu, J. Liu, C. Song, The orientation and stability of the GPCR-Arrestin complex in a lipid bilayer, Scientific reports, 7 (2017) 16985.
[47] A. Ebadi, D. Dastan, M. Azami, A. Karimi, N. Razzaghi-Asl, Molecular Modeling of Human CCR2 Receptor within POPC Lipid Bilayer, Structural Chemistry, 28 (2016) 849-857.
[48] M.H. Khatami, I. Saika-Voivod, V. Booth, All-atom molecular dynamics simulations of lung surfactant protein B: Structural features of SP-B promote lipid reorganization, Biochimica et biophysica acta, 1858 (2016) 3082-3092.
[49] M.H. Khatami, M. Bromberek, I. Saika-Voivod, V. Booth, Molecular dynamics simulations of histidine-containing cod antimicrobial peptide paralogs in self-assembled bilayers, Biochimica et biophysica acta, 1838 (2014) 2778-2787.
[50] J. Zhang, Y. Hou, Y. Wang, C. Wang, X. Zhang, The LBFGS quasi-Newtonian method for molecular modeling prion AGAAAAGA amyloid fibrils, Natural Science, 04 (2012) 1097-1108.
[51] A.G. Bailey, C.P. Lowe, MILCH SHAKE: an efficient method for constraint dynamics applied to alkanes, J Comput Chem, 30 (2009) 2485-2493.
[52] Y. Shan, J.L. Klepeis, M.P. Eastwood, R.O. Dror, D.E. Shaw, Gaussian split Ewald: A fast Ewald mesh method for molecular simulation, J Chem Phys, 122 (2005) 54101.
[53] S.J. Stuart, R. Zhou, B.J. Berne, Molecular dynamics with multiple time scales: The selection of efficient reference system propagators, The Journal of Chemical Physics, 105 (1996) 1426-1436.
[54] K.J. Bowers, D.E. Chow, H. Xu, R.O. Dror, M.P. Eastwood, B.A. Gregersen, J.L. Klepeis, I. Kolossvary, M.A. Moraes, F.D. Sacerdoti, J.K. Salmon, Y. Shan, D.E. Shaw, Scalable Algorithms for Molecular Dynamics Simulations on Commodity Clusters, Proceedings of the 2006 ACM/IEEE SC|06 Conference (SC'06), (2006) p 43.
[55] F. Fogolari, A. Brigo, H. Molinari, Protocol for MM/PBSA molecular dynamics simulations of proteins, Biophys J, 85 (2003) 159-166.
[56] J.A. Ballesteros, H. Weinstein, [19] Integrated methods for the construction of three-dimensional models and computational probing of structure-function relations in G protein-coupled receptors, Receptor Molecular Biology1995, pp. 366-428.
[57] E.S. Tan, J.C. Naylor, E.S. Groban, J.R. Bunzow, M.P. Jacobson, D.K. Grandy, T.S. Scanlan, The molecular basis of species-specific ligand activation of trace amine-associated receptor 1 (TAAR(1)), ACS Chem Biol, 4 (2009) 209-220.
[58] W. Cho, L.P. Taylor, A. Mansour, H. Akil, Hydrophobic residues of the D2 dopamine receptor are important for binding and signal transduction, J Neurochem, 65 (1995) 2105-2115.
[59] M. Michino, T. Beuming, P. Donthamsetti, A.H. Newman, J.A. Javitch, L. Shi, What can crystal structures of aminergic receptors tell us about designing subtype-selective ligands?, Pharmacol Rev, 67 (2015) 198-213.
[60] L. Shi, J.A. Javitch, The binding site of aminergic G protein-coupled receptors: the transmembrane segments and second extracellular loop, Annu Rev Pharmacol Toxicol, 42 (2002) 437-467.